Letter

A Six-Switch Seven-Level Triple-Boost Inverter

Manxin Chen, *Student Member, IEEE*, Poh Chiang Loh, Yongheng Yang, *Senior Member, IEEE*, and Frede Blaabjerg, *Fellow, IEEE*

***Abstract*—Multilevel inverters in renewable applications usually require a high-voltage dc link fed by a front-end dc–dc boost stage. Such a two-stage power conversion, however, increases the switch count, leading to higher costs and power losses. To lower the number of switches, this letter proposes a six-switch inverter, capable of generating a seven-level voltage and a triple-voltage boost. Both features are achieved with only four switches operating at a high frequency while clamped by low-voltage capacitors. The remaining two switches must, however, endure higher voltage stresses but fortunately operate at a much lower frequency. The overall switching losses of the inverter are, thus, significantly reduced. Besides, the inverter shares a common ground between its dc input and ac output, which theoretically helps to eliminate the leakage current, if powered by photovoltaic sources. The operating principles of the inverter have been described and verified through experiments with an 800-W prototype.**

***Index Terms*—Boost multilevel inverter (MLI), common-grounded (CG) structure, low switch count, renewable applications.**

I. Introduction

THE exploitation of renewable energy is important because of environmental concerns. Harvesting renewable energy requires a large number of power converters, among which, multilevel inverters (MLIs) are the most commonly used [1]. MLIs, including the neutral-point-clamped (NPC) and flying-capacitor inverters, have many advantages, including high-quality output voltage, low *dv*/*dt* across the switches, and small output filter [2]. However, when used for the photovoltaic (PV) generation, some forms of voltage boosting for the grid connection are necessary, since the output voltages of most PV arrays are relatively low. One boost option is to cascade many PV modules as a high-voltage string [3], which presently has met many mismatch issues. Alternatively, a front-end dc–dc converter can be added to form a two-stage dc–ac power converter [4]. This power converter, however, uses more switches with accompanied higher costs and power losses. A third option involving the single-stage boost MLIs has, therefore, been deliberated [5]–[15].

One such attempt in [5] achieves its boosted output voltage from a multi-dc link formed by the multiple switched-capacitor cells (SCCs) in series. Its number of switches N_S in each SCC is, however, still comparably high. That prompts Ye *et al.* [6] to introduce another multi-dc link but like Hinago and Koizumi [5], its usage of a rear-end full bridge for generating the desired ac output remains a concern.

It should, however, be pointed out that the reversal of the output-voltage polarity in each half fundamental cycle does not necessarily require a full bridge. One example is in [7], where an SCC-based five-level boost inverter with inherent polarity reversal has been proposed. That inverter, however, demands nine switches with at least four of them conducting simultaneously. The increases in switches are even more noticeable in [8] and [9] at a higher voltage level. It may, therefore, be more appealing to consider the variant in [10], where some switches and their gating circuits in [9], have been replaced by diodes. Despite that, both inverters must have their leakage currents suppressed before they can be suitable for PV applications.

Other MLIs use an active NPC structure to construct either a five-level or a seven-level inverter [11]–[13], whose switch count can further increase if the bidirectional switches are needed [12], [13]. Such an active NPC structure additionally has a low voltage conversion ratio due to its clamping of grounded neutral of its ac output to the midpoint of its dc input [11]. Despite that, MLIs with a common-grounded (CG) connection can result in the minimization of the leakage current, as also demonstrated by the inverters in [14] and [15]. Another feature shared by the MLIs [11]–[15], is the switch count N_S of each inverter being always higher than the number of voltage levels N_{VL}. Certainly, this is an achievement but not as challenging as the rarely attained target of reducing switches per level (i.e., $N_S/N_{\mathrm{VL}}<1$), while yet producing the desired high-voltage boost.

The challenge has now been met in this letter through the proposal of a six-switch (6S) seven-level (7L) inverter with a triple boost (TB) in the output voltage. The three-phase schematic view of the inverter is shown in Fig. 1, where it is powered by a single dc input and conditioned by a shared dc-link capacitor

Manuscript received May 24, 2020; revised June 29, 2020; accepted July 13, 2020. Date of publication July 17, 2020; date of current version September 22, 2020. This work was supported by the University Grants Committee, Hong Kong. *(Corresponding author: Manxin Chen.)*

Manxin Chen and Poh Chiang Loh are with the Department of Electronic Engineering, The Chinese University of Hong Kong, Shatin, Hong Kong (e-mail: mxchen@link.cuhk.edu.hk; pcloh@ee.cuhk.edu.hk).

Yongheng Yang and Frede Blaabjerg are with the Department of Energy Technology, Aalborg University, 9220 Aalborg, Denmark (e-mail: yoy@et.aau.dk; fbl@et.aau.dk).

Color versions of one or more of the figures in this letter are available online at https://ieeexplore.ieee.org.

Digital Object Identifier 10.1109/TPEL.2020.3010010

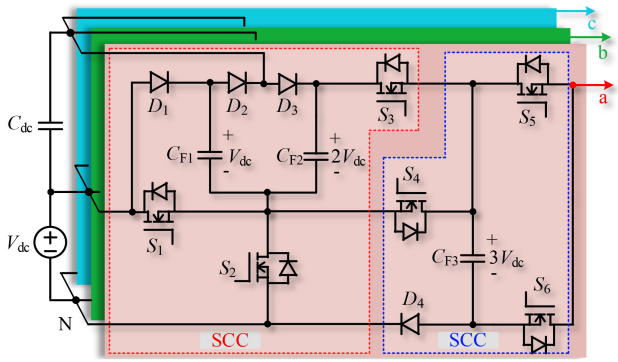

Fig. 1. 6S7LTBI and its three-phase schematic view (terminals *a*, *b*, and *c*).

TABLE I
SWITCHING SIGNALS AND KEY VOLTAGES OF THE 6S7LTBI

States	S_1 ($\overline{S_2}$)	S_3 ($\overline{S_4}$)	S_5 ($\overline{S_6}$)	V_o	V_{CF1}	V_{CF2}	V_{CF3}
I	0	0	0	$-3V_{dc}$	Increase	/	Decrease
II	0	0	1	0	Increase	/	/
III	0	1	0	$-V_{dc}$	Increase	Increase	Decrease
IV	0	1	1	$2V_{dc}$	Increase	Increase	/
V	1	0	0	$-2V_{dc}$	Decrease	/	Decrease
VI	1	0	1	V_{dc}	Decrease	/	/
VII	1	1	0	0	Decrease	Decrease	Increase
VIII	1	1	1	$3V_{dc}$	Decrease	Decrease	Increase

0: switch-OFF; 1: switch-ON; /: No change.

C_{dc}. Throughout the letter, the proposed inverter has been notated as 6S7LTBI and shown to have the following features:

1) a very low switch-per-level ratio (≈0.86);
2) reduced losses achieved by only three switch pairs with one pair operating at the fundamental frequency;
3) common dc-input and ac-output ground and hence a very small leakage current;

These features are systematically explained by first describing the operating states of the 6S7LTBI with a multicarrier pulsewidth modulation (PWM) scheme in Section II. The determination of its parameters and a comparison with other MLIs then follow in Section III. Last, but importantly, the experimental results are given in Section IV. Finally, the conclusion is drawn in Section V.

II. OPERATION OF 6S7LTBI

A. Operating States

The 6S7LTBI consists of three floating capacitors C_{F1}–C_{F3} per phase, whose capacitances, and that of C_{dc}, can be assumed as large enough to keep their respective voltages constant. Among them, C_{F1} and C_{F2} with switches S_1–S_3 and diodes D_1–D_3 form the first SCC, while C_{F3} with switches S_4–S_6 and diode D_4 form the second SCC. Together, they produce eight switching states, as summarized in Table I and Fig. 2. These states, in turn, give rise to an output voltage with seven discrete levels notated as $\pm 3V_{dc}$, $\pm 2V_{dc}$, $\pm V_{dc}$, and 0, where V_{dc} represents the dc input voltage. Conceptually, $2V_{dc}$ and $3V_{dc}$ are the boosted voltages, respectively, associated with C_{F2} in Fig. 2(d) and C_{F2} in series with the dc input in Fig. 2(h). Similarly, $-3V_{dc}$ is obtained by reversing C_{F3} in Fig. 2(a), and $-2V_{dc}$ is achieved by the reverse series connection of the dc input and C_{F3} in Fig. 2(e). These, together with other equivalent circuits in Fig. 2 for generating $\pm V_{dc}$ and 0, show the viability of obtaining seven voltage levels with only six switches.

In practice, the six switches must additionally create the charging and discharging intervals for the three floating capacitors, which in Table I are indicated by their voltages increasing or decreasing. None of the floating capacitive voltages will, hence, drop to zero or increase indefinitely. In other words, the average voltages of the floating capacitors can self-balance around their specified constant values. Likewise, the dc-link capacitor C_{dc} discharges when in states I–IV and charges when in states V–VIII to keep a steady voltage.

Furthermore, in all states, neutral *N* of the ac output has been grounded to the negative terminal of the dc input. The variation of the terminal voltage of the dc source is, therefore, restricted, which in turn, eliminates the leakage current. In addition, unlike the usual seven-level NPC structure, the modulation strategy for the 6S7LTBI needs to create three pairs of complementary gating signals for its six switches, to be demonstrated next.

B. Multicarrier PWM

Three triangular carriers (T_1–T_3) with the same frequency f_s, amplitude E_c, and phase for generating three preliminary independent gating signals are shown in Fig. 3(a). Also shown in the figure is a rectified sinusoidal reference V_{ref} with a peak of A_m. This, together with the amplitude of carriers, gives rise to a modulation index of $M_a = A_m/(3E_c)$. The implementation of the state-selection logic is then given in Fig. 3(b), where the eventual gating signals for the switches (S_1, S_3, and S_5) in Fig. 3(a) are chosen from a lookup table. A notable feature observed with the signals is that the switches S_5 and S_6 are switched at the fundamental frequency to lower the overall switching losses. Other switches, however, have to operate at a high frequency but are fortunately clamped by the low-voltage capacitors, as analyzed in the following section.

III. PERFORMANCE INDEXES

A. Switch Voltage Stresses

From the eight states in Fig. 2, voltage stresses (V_{dsi}, $i = 1$–6) of the six switches are found as

$$V_{ds1} = V_{ds2} = \frac{1}{2} V_{ds3} = \frac{1}{2} V_{ds4} = \frac{1}{3} V_{ds5} = \frac{1}{3} V_{ds6} = V_{dc}. \quad (1)$$

Including voltage stresses (V_{dj}, $j = 1$–4) of the diodes, the total standing voltage (TSV) of all semiconductors in per unit, after normalizing with the maximum output voltage $V_{o\text{-max}}$, is thus

$$\text{TSV} = \left(\sum_{i=1}^{6} V_{dsi} + \sum_{j=1}^{4} V_{dj} \right) \Big/ (n_{vb} V_{dc}) = 6 \quad (2)$$

where $n_{vb} = V_{o\text{-max}}/V_{dc}$ is the voltage-boost ratio.

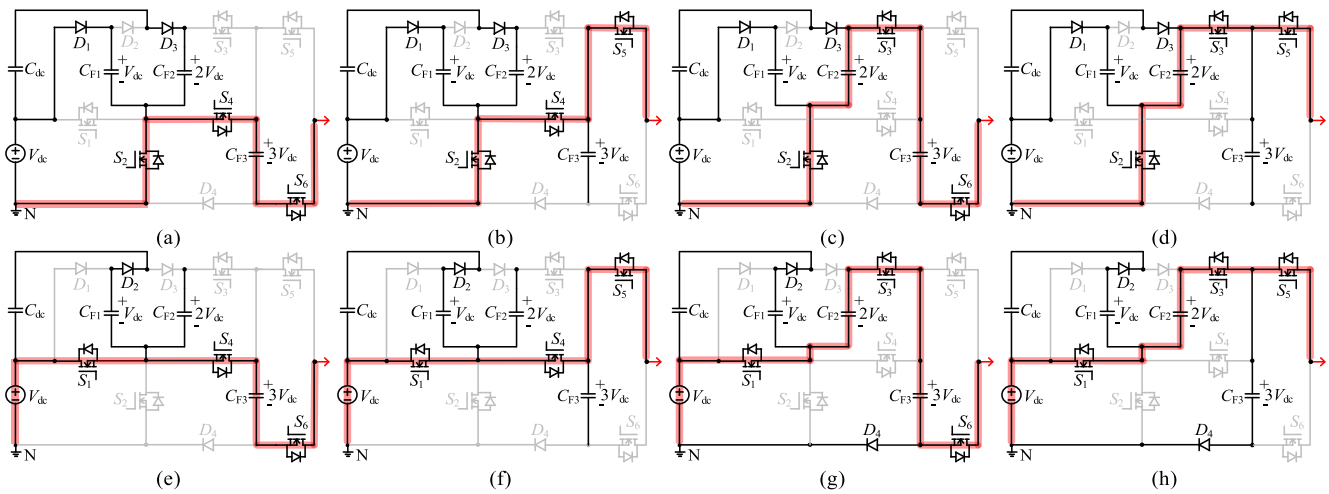

Fig. 2. Equivalent 6S7LTBI when in states I–VIII with the output voltages of (a) $-3V_{\rm dc}$, (b) 0, (c) $-V_{\rm dc}$, (d) $2V_{\rm dc}$, (e) $-2V_{\rm dc}$, (f) $V_{\rm dc}$, (g) 0, and (h) $3V_{\rm dc}$.

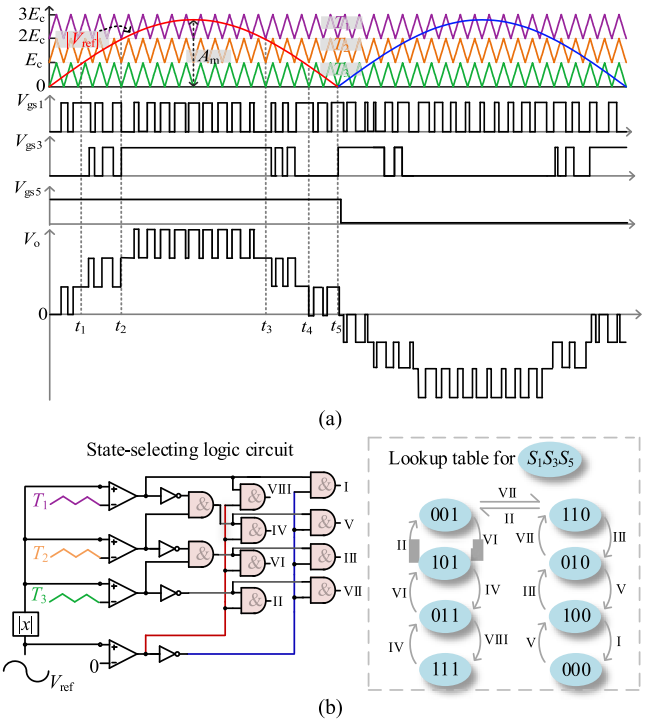

Fig. 3. Illustrations of (a) key PWM waveforms and (b) logics for generating gating signals $V_{\rm gs1}$, $V_{\rm gs3}$, and $V_{\rm gs5}$.

B. Capacitor Voltage Ripples

The peak charging and discharging currents of the floating capacitors depend on voltage difference $\Delta v_{\rm CF}$ between two of them at their starting instant of the parallel connection. It is, therefore, possible to reduce the two peak currents to the acceptable values by keeping the voltage ripples of the floating capacitors small. For C_{F1} and C_{F2}, this is not a major issue since they do not discharge within two consecutive states. They can, therefore, replenish in each switching cycle to maintain a steady voltage with only a small voltage ripple ($\Delta v_{\rm CF1,2}$). The same does not apply to C_{F3}, which continuously discharges to the output over the time span (t_4–t_1), as shown in Fig. 3(a). Its voltage ripple is thus relatively large and expressed as

$$\Delta v_{\rm CF3} = \frac{1}{2C_{F3}} \left| \int_{t_1}^{t_4} \sqrt{2} I_o \sin(\omega t)\, dt \right| \tag{3}$$

where ω and I_o are the angular frequency and rms value of the output current $i_{\rm o}$, respectively.

Assuming a specification of $\Delta v_{\rm CF3} \le 5\% V_{\rm CF3}$, capacitance C_{F3} must hence have a relatively large value and satisfy

$$C_{F3} \ge \frac{10}{3V_{\rm dc}} \left| \int_{t_1}^{t_4} \sqrt{2} I_o \sin(\omega t)\, dt \right|. \tag{4}$$

C. Loss Analyses

The efficiency of the 6S7LTBI mainly depends on the semiconductor losses caused by the currents flowing through them. For that, diodes D_1 and D_3 are noted to conduct the input current $I_{\rm in}$ when in states I–IV. Their average currents I_{d1} and I_{d3} can, thus, be regarded as half of the input current. Similarly, the average current I_{d2} of diode D_2 in states V–VIII can be viewed as $1/2I_{\rm in}$. The differences, however, occur with diode D_4, whose current in states VII and VIII is $I_{\rm in}$–i_o. Its average value can be approximated as $I_{\rm in}$. The determined currents can then be used in the following equation to find the overall conduction losses of the diodes:

$$P_d = \frac{V_F}{2}\left(\frac{I_{\rm in}}{2}\times 3 + \frac{\overline{(I_{\rm in}-i_o)}}{2}\right) \approx \frac{V_F}{2}\left(\frac{I_{\rm in}}{2}\times 4\right) \tag{5}$$

where V_F is the forward voltage drop across each diode.

As for the switches, their conduction losses can be divided into three switch pairs, noting too that only three switches of the 6S7LTBI are conducting at any instant. The first switch pair $\{S_1, S_2\}$ conducts ($I_{\rm in}$–i_o) when in states I–IV and ($I_{\rm in}$+I_{d2}) in states V–VIII. The conduction losses of its switches S_1 and S_2

TABLE II
COMPARISONS WITH EXISTING SINGLE-SOURCE MLIS

MLIs	$N_{\rm VL}$	$N_{\rm S}$	$N_{\rm D}$	$N_{\rm FC}$	TSV	CF with α:		$n_{\rm vb}$	$I_{\rm lk}$ (PV)	Total cost (USD)
						1	2			
[7]	5	9	0	1	4.5	21.25	23.25	2	High	62.29
[8]	9	11	0	2	5.5	26.75	29.5	2	High	75.43
[9]	9	12	0	2	5.25	27.31	28.63	4	High	81.17
[10]	9	8	3	3	5.75	23.44	24.88	4	High	66.30
[11]	7	8	2	2	6	26	32	1	Low (NPC)	65.13
[12]	7	10	0	2	7.33	26.89	31.77	1.5	Low (NPC)	81.69
[13]	7	10	0	1	6	25	29	1.5	Low (NPC)	73.67
[14]	5	7	0	2	5	21	26	1	Low (CG)	64.73
[15]	5	7	2	2	8.5	22.25	26.5	2	Low (CG)	72.21
6S7LTB	7	6	4	3	6	21	23	3	Low (CG)	64.72

The total cost is for a design example based on the devices in Table III.

TABLE III
DEVICES CHOSEN FOR STUDIED MLIS

Volt-str.	Si MOSFETs ($)	Si diode ($)	Driver ($)	C0 ($)
$2V_{o\text{-max}}$	STW30N80K5 (6.38)	/	HCPL-3120 (3.86)	381LX102M400 (6.31)
$4V_{o\text{-max}}/3$	IPW60R125C6 (5.09)	/		
$V_{o\text{-max}}$	FQA30N40 (4.75)	STTH30R04 (3.55)		
$3V_{o\text{-max}}/4$ $2V_{o\text{-max}}/3$	IXFA26N30X3 (3.18)	APT30D30B (2.09)		
$V_{o\text{-max}}/2$ $V_{o\text{-max}}/3$	IRFP250NPBF (2.71)	FFPF30UP20S (1.37)		
$V_{o\text{-max}}/4$	IRLI2910PBF (1.91)	SDT30B100D1 (0.63)		

(Volt-Str. = Voltage Stress)
Unit price ($) from www.digikey.com and may vary with purchase quantities.

can thus be computed using

$$P_{\rm con1} = \frac{R_{\rm on}}{2}\left({I_{\rm in}}^2 + \left(I_{\rm in} + I_{d2}\right)^2\right) \tag{6}$$

where $R_{\rm on}$ represents the same ON-state resistance for all switches.

The same applies to the other switch pairs $\{S_3, S_4\}$ and $\{S_5, S_6\}$, whose conduction losses can be computed using

$$P_{\rm con2} + P_{\rm con3} = R_{\rm on}\left({I_{\rm in}}^2 + {I_o}^2\right). \tag{7}$$

In terms of the switching losses, only switches S_1–S_4 need to be considered since S_5 and S_6 are operating at the fundamental frequency. Moreover, for S_3 and S_4, they switch rapidly only over certain intervals, as depicted by Fig. 3(a). The maximum time that can be occupied by these intervals is half of a fundamental period, divided between the positive and negative half cycles. Therefore, the overall switching losses are calculated by

$$P_{\rm sw} = \frac{(t_r + t_f)\, f_s}{2}\left(V_{\rm dc}\left(I_{ds1} + I_{ds2}\right) + 2V_{\rm dc}\frac{I_{ds3} + I_{ds4}}{2}\right) \tag{8}$$

where t_r and t_f are, respectively, the turn-ON and -OFF times of the switches, and I_{ds1}–I_{ds4} are the average currents through S_1–S_4, respectively.

D. Comparison With Existing MLIs

The numbers of voltage levels, switches, diodes, and floating capacitors ($N_{\rm VL}$, N_S, N_D, and $N_{\rm FC}$) of the 6S7LTBI are compared with those of existing single-source MLIs in Table II. Other parameters compared in the same table are TSV and $n_{\rm vb}$ of the considered MLIs. Returning to $N_{\rm VL}$ and N_S, they particularly inform that the 6S7LTBI uses the least number of switches to produce an output voltage with seven levels or $N_{\rm VL} = 7$, which is thus higher than those in [7], [14], and [15]. Its switch-per-level ratio is very low at around 0.86. Its TSV is not high either and, in fact, smaller than or equal to those of the seven-level inverters [11]–[13]. It is, however, higher than those of the five-level inverters [7], [14], and nine-level inverters [8]–[10]. These compared MLIs, nevertheless, use more switches and hence more gating circuits. A way to consolidate all compared numbers for all the MLIs is thus necessary, which from [10], can be achieved using the following cost function (CF):

$$\mathrm{CF} = N_{\rm Dr} + N_S + N_D + N_{\rm FC} + \alpha \cdot \mathrm{TSV}/n_{\rm vb} \tag{9}$$

where $N_{\rm Dr}$, representing the number of gate drivers, is assumed to be equal to N_S.

Also included in (9) is coefficient α for tuning the weighted cost of selecting different semiconductors (materials such as Si, SiC, or GaN, types such as insulated-gate bipolar transistor (IGBT), or MOSFET, or ratings). With α then set to one and two for the low- and high-cost semiconductors, respectively, CF of each MLI can be computed, as tabulated in Table II. The numbers show that the inverter from [14] and 6S7LTBI have the lowest CF. The lowest CF has, however, not included the influences from floating capacitances, their voltages $V_{\rm CF}$, voltage ripples, and power ratings, which in practice, may affect the total cost of the MLIs. To demonstrate, the monetary costs for all considered MLIs at 1-kW and with $V_{o\text{-max}} = 400$ V are computed, after identifying appropriate semiconductors. For that, Table III lists eight voltage stresses that the switches/diodes of the considered MLIs must endure, followed by the recommended parts and their unit costs. As for the floating capacitors, a quick estimate of their costs starts by choosing a base, which as given in Table III, is a 400-V, 1-mF capacitor $C0$ with unit cost $\$_{C0}$. The estimated cost of each floating capacitor can then be expressed as $V_{\rm CF}/V_{o\text{-max}} \times \$_{C0}$.

The eventual computed monetary costs are given in the last column of Table II, where the MLI from [7] has the lowest monetary cost, even though its CFs are slightly higher than those of the 6S7LTBI. The differences are due to more details accounted when computing the more complex monetary costs. Both CF and monetary costs have, however, undisputedly projected the 6S7LTBI as a low-cost MLI that can produce seven-level switching with only six switches.

Besides the cost, applicability as a renewable PV generator for all MLIs has been deliberated. Beginning with the criterion of $n_{\rm vb}$ larger than unity, MLIs from [11] and [14] are undoubtedly less suitable. Also, among MLIs capable of suppressing leakage current $I_{\rm lk}$ by either adopting the NPC or CG structure, the MLI from [15] produces a five-level output with a gain of two. This is less appealing than the seven-level output with a gain of three obtained from the 6S7LTBI. The 6S7LTBI is, therefore, suitable for interfacing with the low-voltage PV modules while using low-profile output filters.

TABLE IV
COMPONENTS OF THE 800-W INVERTER PROTOTYPE

Voltage ratings	V_{dc}=100 V; $V_{o\text{-}max}$=300 V, 190 Vrms, 800 W
Capacitances	$C_{dc} = C_{F1} = C_{F2} = 220$ μF; $C_{F3} = 4000$ μF
Switches / diodes	SCT3060AL × 6 / C3D20065 × 4

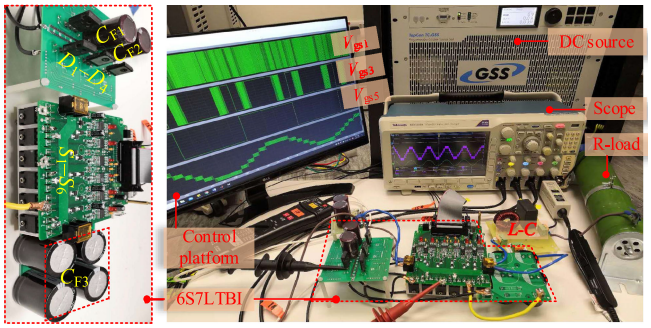

Fig. 4. Photographs of the (a) inverter prototype and (b) testing setup.

However, with only six switches, it does not have redundant states for replacing any unintentionally failed states. Also, like many SCC-based MLIs [9]–[15], the voltage stresses experienced by its semiconductors are nonidentical. Different switches and diodes may be necessary when optimizing its implementation. Finally, its usage of the electrolytic capacitors and diodes to form the SCC may affect the efficiency when supplied by a low input voltage. The 6S7LTBI, therefore, does have some concerns, although its advantages outweigh those concerns.

IV. EXPERIMENTAL RESULTS

An 800-W single-phase 6S7LTBI has been built using the components from Table IV. Its PWM has a carrier frequency of 25 kHz and a modulation ratio of $M_a = 0.9$, while its input has a capacitor added in parallel with the 100-V source (V_{dc}). An output LC filter has then been added between the inverter and resistive load, as in Fig. 4. Fig. 5(a) shows the resulting steady-state output, which clearly has seven distinct voltage levels formed by voltages 100 V, 200 V, and 300 V across C_{F1}–C_{F3}, respectively, as captured by Fig. 5(b). The highest output voltage level is thus 300 V or the achievable n_{vb} is 3, in accordance with the analysis. Concurrently, the capacitors have clamped voltages across the power switches, among which S_5 and S_6 endure the highest clamped voltage but is driven at the fundamental frequency, as seen in Fig. 5(c).

Other results showing the 6S7LTBI step changing from no load to full load and from a modulation index M_a of 0.2–0.6 and then to 0.9 are given in Fig. 5(d) and (e), respectively. Together, they confirm the stable dynamic operations of the 6S7LTBI. As for its ability to manage the reactive power, Fig. 2 shows all its eight states having a bidirectional current path between its input and output. It can, therefore, operate with the nonunity power factor, during which some small amount of energy will return to the source in case of a single-phase system. This expectation, together with supplying the nonlinear load, has been confirmed by the waveforms shown in Fig. 5(f)–(h).

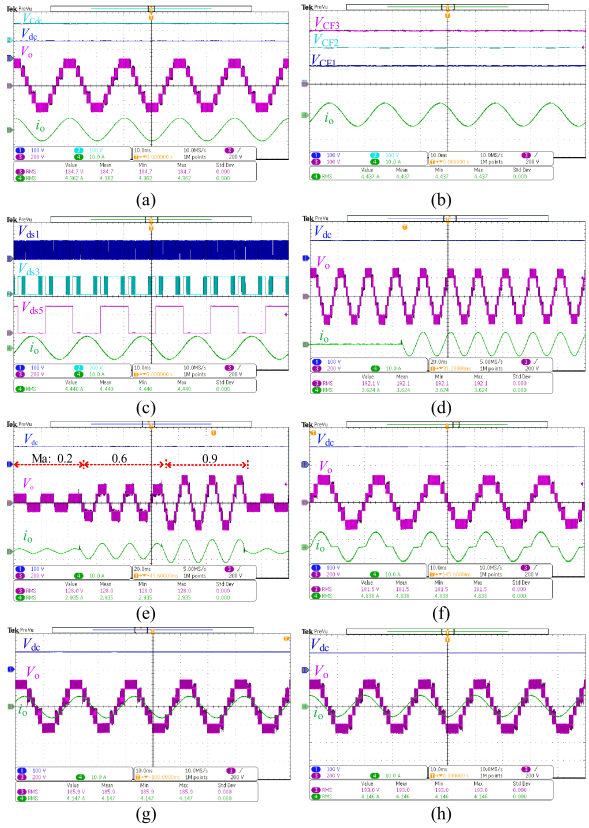

Fig. 5. Experimental results of the 800-W inverter prototype. (a) Voltages of the dc input V_{dc} (100 V/div), dc-link capacitor V_{Cdc} (100 V/div), ac output V_o (200 V/div) and rms 185 V, and ac output current I_o (10 A/div) and rms 4.4 A. (b) Voltages of the floating capacitors V_{CF1}–V_{CF3} (100 V/div). (c) Voltages of the switches V_{ds1} (100 V/div), V_{ds3} (200 V/div), and V_{ds5} (200 V/div). (d) Step change from no load to full load. (e) Performance under a varied M_a. (f)–(h) Operation under a nonlinear, inductive, or capacitive load.

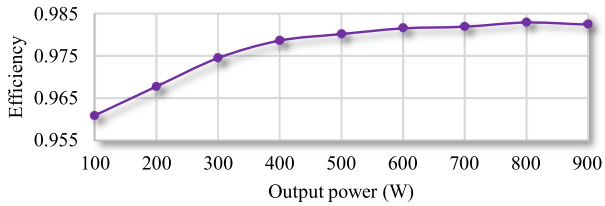

Fig. 6. Measured efficiencies with a 100-V dc input and a 190-Vrms ac output.

Last but importantly, Fig. 6 shows the efficiencies of the 6S7LTBI falling within 97% ± 1.3% at different output powers. Such high efficiencies are undoubtedly due to its low conduction and switching losses, earlier proven theoretically.

V. CONCLUSION

A seven-level inverter with the minimum number of switches has been proposed. Its features include offering a triple voltage-boost and a CG connection for eliminating the leakage current in a PV system. It also uses only a simple gate-driving pattern, designed to reduce the conduction and switching losses. These features have collectively been compared with the existing inverters and tested through experiments, which indeed record a high voltage gain and a high efficiency.

REFERENCES

[1] K. K. Gupta, A. Ranjan, P. Bhatnagar, L. K. Sahu, and S. Jain, "Multilevel inverter topologies with reduced device count: A review," *IEEE Trans. Power Electron.*, vol. 31, no. 1, pp. 135–151, Jan. 2016.

[2] J.-S. Lai and F. Z. Peng, "Multilevel converters-a new breed of power converters," *IEEE Trans. Ind. Appl.*, vol. 32, no. 3, pp. 509–517, May/Jun. 1996.

[3] S. B. Kjaer, J. K. Pedersen, and F. Blaabjerg, "A review of single-phase grid-connected inverters for photovoltaic modules," *IEEE Trans. Ind. Appl.*, vol. 41, no. 5, pp. 1292–1306, Sep./Oct. 2005.

[4] S. K. Kuncham, K. Annamalai, and N. Subrahmanyam, "A two-stage t-type hybrid five-level transformerless inverter for PV applications," *IEEE Trans. Power Electron.*, vol. 35, no. 9, pp. 9510–9521, Sep. 2020.

[5] Y. Hinago and H. Koizumi, "A switched-capacitor inverter using series/parallel conversion with inductive load," *IEEE Trans. Ind. Electron.*, vol. 59, no. 2, pp. 878–887, Feb. 2012.

[6] Y. Ye, K. W. E. Cheng, J. Liu, and K. Ding, "A step-up switched-capacitor multilevel inverter with self-voltage balancing," *IEEE Trans. Ind. Electron.*, vol. 61, no. 12, pp. 6672–6680, Dec. 2014.

[7] N. Sandeep, J. S. M. Ali, U. R. Yaragatti, and K. Vijayakumar, "A self-balancing five-level boosting inverter with reduced components," *IEEE Trans. Power Electron.*, vol. 34, no. 7, pp. 6020–6024, Jul. 2019.

[8] J. S. M. Ali and V. Krishnasamy, "Compact switched capacitor multilevel inverter (CSCMLI) with self-voltage balancing and boosting ability," *IEEE Trans. Power Electron.*, vol. 34, no. 5, pp. 4009–4013, May 2019.

[9] N. Sandeep, J. S. M. Ali, U. R. Yaragatti, and K. Vijayakumar, "Switched-capacitor-based quadruple-boost nine-level inverter," *IEEE Trans. Power Electron.*, vol. 34, no. 8, pp. 7147–7150, Aug. 2019.

[10] J. Liu, W. Lin, J. Wu, and J. Zeng, "A novel nine-level quadruple boost inverter with inductive-load ability," *IEEE Trans. Power Electron.*, vol. 34, no. 5, pp. 4014–4018, May 2019.

[11] Y. P. Siwakoti, A. Mahajan, D. J. Rogers, and F. Blaabjerg, "A novel seven-level active neutral-point-clamped converter with reduced active switching devices and dc-link voltage," *IEEE Trans. Power Electron.*, vol. 34, no. 11, pp. 10492–10508, Nov. 2019.

[12] S. S. Lee and K.-B. Lee, "Dual-T-type seven-level boost active-neutral-point-clamped inverter," *IEEE Trans. Power Electron.*, vol. 34, no. 7, pp. 6031–6035, Jul. 2019.

[13] M. J. Sathik, N. Sandeep, and F. Blaabjerg, "High gain active neutral point clamped seven-level self-voltage balancing inverter," *IEEE Trans. Circuits Syst. II, Express Briefs*, to be published.

[14] F. B. Grigoletto, "Multilevel common-ground transformerless inverter for photovoltaic applications," *IEEE Trans. Emerg. Sel. Topics Power Electron.*, to be published.

[15] R. Barzegarkhoo, Y. P. Siwakoti, and F. Blaabjerg, "A new switched-capacitor five-level inverter suitable for transformerless grid-connected applications," *IEEE Trans. Power Electron.*, vol. 35, no. 8, pp. 8140–8153, Aug. 2020.